Polymer nanoimprinting using an anodized aluminum mold for structural coloration

Tatsuya Kikuchi*, Osamu Nishinaga, Shungo Natsui, and Ryosuke O. Suzuki
Faculty of Engineering, Hokkaido University
N13-W8, Kita-ku, Sapporo, Hokkaido, 060-8628, Japan

*Corresponding author: Tatsuya Kikuchi
TEL: +81-11-706-6340
FAX: +81-11-706-6342
E-mail: kiku@eng.hokudai.ac.jp

Highlights

Highly ordered aluminum dimple arrays are fabricated via etidronic acid anodizing.

The ordered dimple arrays display structural coloration with a rainbow distribution.

Aluminum nanostructures can be transferred to polymers via nanoimprinting.

The nanostructured polymer surfaces also exhibit structural coloration.

Abstract

Polymer nanoimprinting of submicrometer-scale dimple arrays with structural coloration was demonstrated. Highly ordered aluminum dimple arrays measuring 530 to 670 nm in diameter were formed on an aluminum substrate via etidronic acid anodizing at 210 to 270 V and subsequent anodic oxide dissolution. The nanostructured aluminum surface led to bright structural coloration with a rainbow spectrum, and the reflected wavelength strongly depends on the angle of the specimen and the period of the dimple array. The reflection peak shifts gradually with the dimple diameter toward longer wavelength, reaching 800 nm in wavelength at 670 nm in diameter. The shape of the aluminum dimple arrays were successfully transferred to a mercapto-ester ultra-violet curable polymer via self-assembled monolayer coating and polymer replications using a nanoimprinting technique. The nanostructured polymer surfaces with positively and negatively shaped dimple arrays also exhibited structural coloration based on the periodic nanostructure, and reflected light mostly in the visible region, 400-800 nm. This nanostructuring with structural coloration can be easily realized by simple techniques such as anodizing, SAM coating, and nanoimprinting.

Keywords: Anodizing; Anodic Porous Alumina; Etidronic Acid; Structural Coloration; Nanoimprinting

1. Introduction

Anodic porous alumina possesses characteristic nanofeatures, including highly ordered porous structures with high-aspect ratio nanopores measuring several tens or hundreds of nm in diameter, and can easily be fabricated via aluminum anodizing in several appropriate acidic electrolyte solutions [1-4]. Because it is difficult to obtain such similar high-aspect ratio porous materials by other techniques, anodic porous alumina has been widely investigated by researchers in nano-science and engineering applications, such as fundamentals [5-7], nanotemplates [8-11], optical devices [12-14], sensors [15-17], and catalysts [18-20].

For anodic porous alumina formation by anodizing, the following three acid groups have been reported to date: a) inorganic electrolytes, including sulfuric [21,22], sulfamic [23], selenic [24,25], phosphoric [26,27], and chromic acid [28,29]; b) carboxylic electrolytes, including oxalic [30], malonic [31], tartaric [32], glycolic [33], tartronic [34], citric [35], malic [36], formic [37], ketoglutaric [38], acetonedicarboxylic [38], and acetylenedicarboxylic acid [39]; and c) oxocarbonic electrolytes, including squaric [40], croconic [41], and rhodizonic acid [41]. In particular, anodizing in sulfuric, selenic, oxalic, malonic, tartaric, and phosphoric acid solutions under the appropriate electrochemical conditions causes self-ordering growth of the porous alumina [1,2,42]. Accordingly, highly ordered anodic porous alumina with a high aspect ratio has been successfully obtained on aluminum substrates. However, the cell diameter (interpore distance) of the porous alumina formed in these electrolyte solutions is limited to up to approximately 500 nm in diameter at the corresponding anodizing voltage of 200 V [1]. Therefore, a novel high-voltage electrolyte is required for the self-ordering of porous alumina with large-scale cell diameters.

Recently, we reported a new self-ordering electrolyte for anodic porous alumina fabrication, etidronic acid (1-hydroxyethane-1,1-diphosphonic acid, $CH_3C(OH)[PO(OH)_2]_2$) [43]. Etidronic acid anodizing at 210-270 V under the appropriate temperatures resulted in the formation of anodic porous alumina that exhibited self-ordering behavior, and periodic porous alumina with cell sizes of 530-670 nm was successfully fabricated. A periodic dimple array corresponding to the bottom shape of the ordered porous alumina was also fabricated on the aluminum substrate via selective dissolution of the anodic oxide. During the aluminum dimple formation on the aluminum substrate, we found that the nanostructured aluminum surface led to bright structural coloration with a rainbow spectrum including violet, blue, light blue, green, yellow, orange, and red hues. This structural coloration is not based on the thin film interference but rather the nanostructured aluminum surface with the periodic submicrometer-scale dimple array. Therefore, the ordered aluminum nanostructure, namely the structural coloration, may easily be transferred to other materials including polymers via nanoimprinting [44-46].

The aim of the current study was to establish a technique for the structural coloration via electrochemical nanofabrication and nanoimprinting. We describe a novel

structural coloration approach of aluminum nanostructuring based on etidronic acid anodizing and subsequent polymer nanoimprinting. Highly ordered dimple arrays with 530-670 nm periodic structures were fabricated via etidronic acid anodizing, and the corresponding structural coloration was investigated by optical reflectance spectroscopy. We demonstrated the transfer of the nanostructure to the polymers for the structural coloration via nanoimprinting using nanostructured aluminum molds. The effects of the conditions of anodizing and nanoimprinting on the behavior of the resulting structural coloration were investigated.

2. Experimental

2.1 Pretreatment of the aluminum specimens

High-purity aluminum plates (99.999 wt%, 0.25-1.0 mm thick, GoodFellow, UK) were cut into 20 mm × 10 mm specimens with handles. The aluminum specimens were ultrasonically degreased in a C_2H_5OH solution for 10 min, and then the lower halves of the handles of the specimens were coated with silicone resin (KE45W, Shin-Etsu Chemical, Japan). After solidification of the resin, the specimens were electropolished in a 13.6 M CH_3COOH/2.56 M $HClO_4$ (78 vol% CH_3COOH/22 vol% 70%-$HClO_4$) mixture solution at a constant cell voltage of U = 28 V for 1-5 min. A high-purity aluminum plate was used as the cathode, and the solution was slowly stirred with a magnetic stirrer during electropolishing.

2.2 Fabrication of highly ordered dimple arrays on the aluminum

The electropolished specimens were immersed in a 0.3 M etidronic acid solution (Sigma-Aldrich, USA, T = 293-313 K) and were anodized at a constant cell voltage of U = 210-270 V for up to 16 h. During the initial stage of etidronic acid anodizing, the voltage was increased linearly for 2.5 min and then was held at each voltage to prevent burning due to localized breakdown under the high electric field. A platinum plate was used as the cathode, and the solution was vigorously stirred during the etidronic acid anodizing. To compare the highly ordered nanostructures with the disordered nanostructures, aluminum specimens were also anodized in a 0.2 M ketoglutaric acid solution (HOOC-CO-$(CH_2)_2$-COOH, Kanto Chemical, Japan, T = 293 K) at 270 V for 16 h. The specimens were then immersed in a 0.20 M CrO_3/0.51 M H_3PO_4 mixture solution (T = 353 K) to selectively dissolve the anodic porous alumina on the aluminum substrate. The bottoms of the anodic porous alumina were exposed to the surface by selective oxide dissolution, and the nanostructured aluminum specimens were termed “aluminum dimple arrays”. High-purity aluminum rods (99.99 wt%, 5.0-10.0 mm in diameter, Kojundo Chemical Laboratory, Japan) were also anodized for the fabrication of the aluminum dimple arrays on a curved surface.

2.3 Nanoimprinting using nanostructured aluminum molds

The nanostructured aluminum specimens were immersed in a

tetradecylphosphonic acid (TDPA, $CH_3(CH_2)_{13}P(O)(OH)_2$, Sigma-Aldrich, USA) ethanol solution (5.3 mg TDPA /10 mL C_2H_5OH, room temperature) for 2 days to form a self-assembled monolayer (SAM) on the aluminum surface. After SAM coating, the shape of the aluminum dimple array formed by anodizing was transferred to an elastomeric polydimethylsiloxane (PDMS, Sylgard 184, Dow Corning, USA) polymer via replica molding. The mixture of pre-polymer and curing agent was kept at room temperature for 2 days or at 353 K for 120 min to cure the polymer. In addition, the following PDMS composites were also cured for the fabrication of colored PDMS polymers: a) PDMS/TiO_2 nanoparticles (99.99 wt%, PT-401M, average particle size: 70 nm, Ishihara Sangyo Kaisha, Japan) and b) PDMS/multi-walled carbon nanotube (MWCNT, >95 wt%, diameter: 6-9 nm, Sigma-Aldrich) nanocomposites. The weight ratios of base to curing reagent were fixed at 10 (30 mL) : 1 with/without 1.0 g TiO_2 nanoparticles or 1.0 g MWCNTs.

After PDMS curing, the shape of the negative structure on the PDMS mold was again transferred to a mercapto-ester ultra-violet (UV) curable polymer (NOA60, Norland Products, USA) via a second replica molding. For the second molding, the pre-polymer was coated on the PDMS negative mold and covered with a thin slide glass under UV irradiation (365 nm, handheld UV curing lamp, Edmund Optics, USA) for 60 min. Curing photopolymers with ordered dimple arrays were fabricated via two successive replica moldings, as described above.

2.4 Characterization of the nanostructured specimens

The surfaces of the nanostructured aluminum specimens and polymers were examined by field-emission scanning electron microscopy (FE-SEM, JIB-4600F/HKD, JEOL, Japan). For polymer observation, a thin platinum electro-conductive layer was coated on the specimens using a magnetron sputter coater (MSP-1S, Vacuum Device, Japan). Optical reflectance measurements from the nanostructured aluminum and polymers were performed using a PC-controlled multi-channel spectrometer (USB2000+, Ocean Optics, USA). The specimens were set in the perpendicular position of a white light source (HL-2000, Ocean Optics) through an optical fiber and were rotated by a θ-axis stage (SKIDS-60YAW(θz), SIGMAKOKI, Japan) from 0 to 50.0°. The reflectance of the rotated specimens was measured at visible and infrared regions of 400-900 nm.

3. Results and discussion

3.1 Nanostructured aluminum surfaces and their structural coloration

Etidronic acid anodizing at three voltages was carried out to understand the effect of the cell diameter of the aluminum dimple arrays on the structural coloration. Fig. 1 shows the changes in the current density, j, at several voltages, U = 210-270 V, during constant voltage anodizing in a 0.3 M etidronic acid solution (T = 293-313 K). To form the highly ordered anodic porous alumina with large-scale cell diameters, three

appropriate anodizing voltages and the corresponding solution temperatures to prevent burning were selected for anodizing [43]. At U = 270 V and T = 293 K (Fig. 1a), the current density increased rapidly to j = 100 Am^{-2} during the initial period and then decreased gradually with anodizing time. This current-time transient corresponds to the formation of anodic porous alumina during constant voltage anodizing: the nanopore formation in the barrier anodic oxide and subsequent growth of the porous layer. The current density increased with decreasing voltage (Figs. 1b and 1c) due to the active dissolution of the anodic oxide at the pore bottom during high temperature anodizing. Accordingly, the current density at 210 V during the initial stage was four-times larger than that at 270 V. Namely, the growth rate of the anodic porous alumina also increased with voltage decreasing. The low voltage anodizing was completed early due to rapid and sufficient growth of the porous alumina.

After constant voltage anodizing, the anodic porous alumina was completely dissolved from the aluminum substrate via selective chemical dissolution. Therefore, the bottom shape of the anodic porous alumina was exposed to the surface [25,47]. Fig. 2 shows the surface appearance of the specimens anodized at a) U = 210 V, b) 240 V, and c) 270 V in etidronic acid solution after selective oxide dissolution. Each aluminum surface clearly shows bright structural colors that include blue, green, yellow, and red hues. The non-uniformity of the structural coloration shown in Fig. 2a) though 2c) is due to the slight distortion of the aluminum substrate that is caused when cutting the specimens.

Fig. 2d) shows the surface of the specimen anodized at 270 V in a ketoglutaric acid solution to be compared with the surface of the specimen anodized in etidronic acid solution. Ketoglutaric acid anodizing can be achieved under high voltage conditions, similar to etidronic acid anodizing. Therefore, the aluminum specimen was anodized in a 0.2 M ketoglutaric acid at 270 V for 16 h, and then the anodic oxide was completely removed from the substrate. However, the aluminum surface obtained by ketoglutaric acid anodizing exhibited monochromatic white-gray coloring without a rainbow distribution, in contrast to etidronic acid anodizing. A similar light-gray coloration was observed at different viewing angles, and the structural coloration was not generated due to ketoglutaric acid anodizing. The differences in the surface appearances may be caused by the regularity of the dimple array formed on the aluminum substrate. The detailed nanostructures of these exposed aluminum surfaces were examined using SEM.

Fig. 3 shows SEM images of the exposed aluminum surface after etidronic acid anodizing at a) U = 210 V, b) 240 V, and c) 270 V and selective oxide dissolution. Highly ordered aluminum dimple arrays with ideal cell arrangements were successfully obtained via each etidronic acid anodizing. The average cell diameter of the dimples increased with the anodizing voltage, and periodic dimples measuring a) 530 nm at 210 V, b) 600 nm at 240 V, and c) 670 nm at 270 V in diameter were fabricated on the aluminum substrate. During typical self-ordering of anodic porous alumina, cell diameter increases linearly with the anodizing voltage [1]. These linear relations are

consistent with etidronic acid anodizing, as described above.

Fig. 4 shows an SEM image of the exposed aluminum surface anodized in 0.2 M ketoglutaric acid at 270 V, as shown in Fig. 2d. In contrast to Fig. 3, disordered dimple arrays corresponding to the bottom shape of the disordered anodic porous alumina can be observed by ketoglutaric acid anodizing. Each dimple resembles a combination of circular- and polygon-like shapes. In addition, many white defects were formed at the junctions of each dimple, such as at the fourth and fifth points. The diameters of the disordered dimples varied widely between 415 nm and 1000 nm, as observed based on the SEM images. The average diameter was calculated as approximately 700 nm, which is slightly larger than that obtained by etidronic acid anodizing at the same voltage. Such disordered anodic porous alumina formations have also been observed for the anodizing of other organic acid electrolytes, such as malic and squaric acid solutions [36,40]. These ordered and disordered aluminum dimple arrays fabricated by etidronic and ketoglutaric acid anodizing were used for optical reflectance measurements.

Fig. 5a shows the change in the reflection, R, of the electropolished aluminum surface on the vertical position with wavelength, λ, under white light irradiation. The reflection spectrum is similar to a Gaussian distribution with a peak at approximately 610 nm wavelength. This spectrum becomes the standard distribution for the optical measurements on the nanostructured aluminum surfaces under white light irradiation. The changes in the reflection of the nanostructured aluminum surfaces formed by ketoglutaric acid anodizing according to wavelength are shown in Fig. 5b. During the reflection measurements, the nanostructured aluminum specimen was rotated from 25.0° to 45.0° by a θ-axis stage. The shape of the reflection spectrum at 25.0° was similar to that obtained from the electropolished aluminum, as shown in Fig. 5a. Although the reflection corresponding to wavelengths between approximately 550 nm and 900 nm decreased slightly with increased specimen angles, the surface reflected light made up of the entire visible spectrum in all cases. In fact, white-gray hues were observed from the exposed aluminum specimens at all angles. Namely, the white-gray coloring of the nanostructured aluminum surfaces formed by ketoglutaric acid anodizing resulted in the reflection at wavelengths across the entire visible spectrum. Therefore, such disordered microstructures with submicrometer-scale dimple arrays do not exhibit the selective light reflection based on interference.

Fig. 6 shows the changes in the reflection spectrums of the nanostructured aluminum specimens fabricated by etidronic acid anodizing at a) U = 210 V for D = 530 nm, b) 240 V for 600 nm, and c) 270 V for 670 nm. At 210 V for 530 nm (Fig. 6a), the reflection spectrum shows a broad peak at the lowest angle of 25.0°, and the center position of the peak is not clear. The peak becomes clearer with increased rotation angles of the specimen, and the position of the peak shifts gradually with the angle toward longer wavelengths. Namely, selective color reflection based on the ordered aluminum dimple arrays was observed upon rotating the specimen. This structural coloration is due to an interference shift based on the change of the reflection intervals

of the ordered dimple arrays by the rotation of the specimen, as shown in Figs. 6d and 6e. Increasing the anodizing voltage, i.e., increasing the cell diameter of the dimple arrays, led to notable shifts in each peak toward longer wavelengths (Figs. 6b and 6c). These optical measurements indicate that the structural coloration strongly depends on the cell diameter of the ordered dimple arrays on the aluminum substrate. Therefore, the optimal cell diameter should be selected for the structural coloration for visible light spectrum, especially short (< 500 nm) and long (> 700 nm) wavelength regions.

Structural coloration based on periodic nanostructures occurs often in biological systems, such as in morpho butterfly wings and the bodies of buprestidae [48-49]. Structural coloration achieved using nanofabrication has been recently reported by several research groups [50-51]; however, complicated and expensive techniques are needed for the fabrication of periodic nanostructures. An important advantage of our structural coloration is that the process consists of only simple techniques including anodizing and chemical dissolution.

The nanostructuring of aluminum surfaces for structural coloration can be applied not only to flat plates but also to three-dimensional curved surfaces, such as rods, because anodizing allows for the ease formation of highly ordered dimple arrays on the curved surfaces. Fig. 7 shows the surface appearance of the 5.0-mm and 10.0-mm diameter aluminum rods, which were a) electropolished and b) anodized in an etidronic acid solution after selective oxide dissolution. Bright structural coloration with a rainbow distribution was successfully achieved on the aluminum rods via self-ordering anodizing and subsequent oxide dissolution. Such nanostructured aluminum rods can be employed in roll-to-roll nanoimprinting for the fabrication of nanostructured polymers and other materials, as described in the next section.

3.2 Polymer nanoimprinting using nanostructured aluminum molds

Nanostructured polymers with structural coloration were fabricated via nanoimprinting based on UV polymer curing using an elastomeric PDMS mold. Fig. 8 shows photographs of the typical stages involved in the fabrication of the polymer dimple arrays via the nanoimprinting technique. Before nanoimprinting, phosphonic acid-based SAM (TDPA) was coated on the nanostructured aluminum surface (Fig. 8a) [52-53]. In this procedure, the nanostructured aluminum specimen was immersed in a TDPA ethanol solution for 2 days. Nanoimprinting without the SAM layer could not be achieved due to the high adhesion of nanostructured aluminum specimen to the curing PDMS.

A nanostructured aluminum specimen with the SAM layer was placed in the center of a Petri dish, and then the PDMS prepolymer was poured into the Petri dish (Fig. 8b). The PDMS curing polymer was carefully removed from the Petri dish after curing, and then the nanostructured aluminum specimen was also carefully removed from the PDMS polymer (Fig. 8c). The negative shape of the dimple array, namely a nanodot array, was transformed to the PDMS curing polymer, but the structural coloring

was not observed from the PDMS polymer due to its high transparency (Fig. 8c). The rough edges formed by the meniscus of the PDMS polymer were cut using a knife, and the square-shaped PDMS negative mold was obtained. A UV curable liquid photopolymer (NOA60) was applied to the PDMS negative mold and then exposed to UV light through a glass slide for 1 h (Fig. 8d). After the UV curing, the cured polymer was carefully removed from the PDMS negative mold (Fig. 8e). The nanoimprinting photopolymer with the original shaped-dimple array was obtained on the glass slide. However, little structural coloration was observed from the polymer surface due to its high transparency (Fig. 8e). Therefore, thin platinum coating on the polymer surface was carried out via magnetron sputtering (Fig. 8f). Structural coloration similar to the original nanostructured aluminum surface was clearly observed from the nanostructured polymer on the glass (Fig. 8f). In summary, a dimple array structure could be transferred to a polymer via a nanoimprinting method that incorporated SAM coating, PDMS negative mold formation, and UV photopolymer curing, as shown in Fig. 8a through 8f.

Fig. 9a shows an SEM image of the aluminum surface with a master dimple array after PDMS nanoimprinting. The highly ordered dimple array without any deformation or defect can be observed on the aluminum surface after nanoimprinting. Therefore, the nanostructured aluminum mold can also be used as the master pattern for further nanoimprinting. Fig. 9b shows an SEM image of the nanostructured surface on the UV curable polymer replica fabricated by nanoimprinting, as shown in Fig. 8f. Comparing Fig. 9b with Fig. 3c, the interface between each dimple on the polymer surface is slightly unclear, and the diameter of each dimple is smaller than that of the aluminum master mold. This is may be due to slight deformations of the PDMS negative mold and the UV curable polymer during the curing and removal steps. Although several defects were observed in Fig. 9b, the ordered dimple array could be able to be transferred to the UV curable polymer surface via nanoimprinting.

Fig. 10a and 10b show changes in the reflection from the surface of the UV curable polymer replica a) before and b) after thin platinum coating. For these optical measurements, the intensity of the reflection of the each specimen is reported under the same conditions. For the polymer replica without platinum coating (Fig. 10a), little structural coloration was observed at 15.0-40.0° due to its high transparency, as shown in Fig. 8e. After platinum coating of the polymer replica (Fig. 10b), the light is strongly reflected from the platinum-coated dimple array on the polymer replica, and clear structural coloration can be observed by rotating the specimen. Although the shape of the reflection spectrum is slightly different from the master aluminum pattern due to slight deformations of PDMS mold and the UV photopolymer, structural coloration was successfully transferred to the polymer replica via nanoimprinting.

Structural coloration is generated not only in dimple arrays but also in nanodot array corresponding to the negative shape of the dimple array. Fig. 10c shows changes in the reflection from the backside of the polymer replica through the slide glass.

Although the intensities of the reflection at each angle are less than half of the intensities measured at the surface, similar structural coloration was also measured from the backside of the polymer replica. This decrease in reflection occurs because the white light and reflected light pass through the slide glass and the curable photopolymer during optical measurements.

PDMS negative molds with nanodot arrays exhibit non-structural coloration due to their high transparency, as shown in Fig. 8c. However, colored PDMS polymers exhibit structural coloring from their highly reflective surfaces. Fig. 11 demonstrates the structural coloration of colored PDMS polymers with nanodot arrays. White PDMS/TiO_2 nanoparticle composites were prepared by the dispersion of TiO_2 nanoparticles into PDMS prepolymers and subsequent curing (Fig. 11a). However, structural coloration was not observed from the nanostructured surfaces of the white PDMS/TiO_2 composites due to the strong reflection of all wavelengths of light from the white PDMS substrate. Similarly, black PDMS/MWCNT composites were fabricated by the dispersion of MWCNTs into PDMS prepolymers and subsequent curing (Fig. 11b). The nanostructured black PDMS/MWCNT composites clearly exhibited rainbow color distributions based on the nanodot arrays. Therefore, structural coloration was transferred to the various colored PDMS polymers via nanoimprinting using PDMS prepolymer/nanomaterial composites. Colored PDMS with structural coloration can be employed in various optical applications.

4. Conclusions

We demonstrated bright structural coloration via etidronic acid anodizing and the transfer of nanostructures to PDMS and UV curable polymers via nanoimprinting. Etidronic acid anodizing at 210-270 V induced the formation of highly ordered dimple arrays measuring 530 to 670 nm in diameter on aluminum plates and rods and the structural coloration of the submicrometer-scale ordered dimple arrays. The reflection peaks at each angle strongly depend on the period of the dimple array, and the peak shifts gradually with the dimple diameter toward longer wavelength, reaching 800 nm in wavelength at 670 nm in diameter. Structural coloration was not observed on the nanostructured aluminum surfaces formed by ketoglutaric acid anodizing due to its disordered nanostructure.

The shape of the nanostructured aluminum dimple array was successfully transferred to a mercapto-ester-based photopolymer via TDPA-SAM coating, PDMS negative mold formation, and photopolymer curing. Structural coloration was also observed on the nanostructured polymer surface, and the nanostructured surface reflected light mostly in the visible region, 400-800 nm. The reflection strength from the platinum-coated polymer increased with respect to that of the original polymer without a platinum layer. In addition, nanodot polymer arrays, which are negative structures of the dimple polymer arrays, also exhibited structural coloration of the surface. A black PDMS negative mold also exhibited structural coloration. These nanostructured

polymers, including PDMS and UV curable polymers, can be used for various optical applications.

Acknowledgments

This study was conducted at Hokkaido University and was supported by the "Nanotechnology Platform" Program of the Ministry of Education, Culture, Sports, Science, and Technology (MEXT), Japan. The work was financially supported by the Japan Society for the Promotion of Science (JSPS) "KAKENHI" and Toyota Physical & Chemical Research Institute Scholars.

References

1) W. Lee, S.J. Park, Porous anodic aluminum oxide: anodization and templated synthesis of functional nanostructures, Chem. Rev. 114 (2014) 7487-7556.
2) G.D. Sulka, Highly ordered anodic porous alumina formation by self-organized anodizing, in: A. Eftekhari (Ed.), Nanostructured Materials in Electrochemistry, Wiley-VCH, 2008, pp. 1-116.
3) F. Li, L. Zhang, R.M. Metzger, On the growth of highly ordered pores in anodized aluminum oxide, Chem. Mater. 10 (1998) 2470-2480.
4) G.E. Thompson, Porous anodic alumina: fabrication, characterization and applications, Thin Solid Films 297 (1997) 192-201.
5) I.A. Vrublevsky, A.I. Jagminas, K.V. Chernyakova, Re-Anodizing Technique as a Method of Investigation of Thermally Activated Defects in Anodic Alumina Films, J. Electrochem. Soc. 160 (2013) C285-C290.
6) H. Han, S.J. Park, J.S. Jang, H. Ryu, K.J. Kim, S. Baik, W. Lee, In Situ Determination of the Pore Opening Point during Wet-Chemical Etching of the Barrier Layer of Porous Anodic Aluminum Oxide: Nonuniform Impurity Distribution in Anodic Oxide, ACS Appl. Mater. Interfaces 5 (2013) 3441-3448.
7) I. Vrublevsky, K. Chernyakova, A. Bund, A. Ispas, U. Schmidt, Effect of anodizing voltage on the sorption of water molecules on porous alumina, Appl. Surf. Sci. 258 (2012) 5394-5398.
8) T. Yanagishita, K. Nishio, H. Masuda, Fabrication of metal nanohole arrays with high aspect ratios using two-step replication of anodic porous alumina, Adv. Mater. 17 (2005) 2241-2243.
9) T. Yanagishita, K. Yasui, T. Kondo, Y. Kawamoto, K. Nishio, H. Masuda, Antireflection polymer surface using anodic porous alumina molds with tapered holes, Chem. Lett. 36 (2007) 530-531.
10) M. Steinhart, J.H. Wendorff, A. Greiner, R.B. Wehrspohn, K. Nielsch, J. Schilling, J. Choi, U. Gösele, Polymer nanotubes by wetting of ordered porous templates, Science 296 (2002) 1997.
11) K Nielsch, F Müller, AP Li, U Gösele, Uniform nickel deposition into ordered alumina pores by pulsed electrodeposition, Adv. Mater. 12 (2000) 582-586.

12) I. Mikulskas, S. Juodkazis, R. Tomasiūnas, J.G. Dumas, Aluminum oxide photonic crystals grown by a new hybrid method, Adv. Mater. 13 (2001) 1574-1577.
13) A. Yamaguchi, K. Hotta, N. Teramae, Optical waveguide sensor based on a porous anodic alumina/aluminum multilayer film, Anal. Chem. 81 (2008) 105-111.
14) W.L. Xu, M.J. Zheng, S. Wu, W.Z. Shen, Effects of high-temperature annealing on structural and optical properties of highly ordered porous alumina membranes, Appl. Phys. Lett. 85 (2004) 4364-4366.
15) G. Gorokh, A. Mozalev, D. Solovei, V. Khatko, E. Llobet, X. Correig, Anodic formation of low-aspect-ratio porous alumina films for metal-oxide sensor application, Electrochim. Acta 52 (2006) 1771-1780.
16) J.H. Yuan, K. Wang, X.H. Xia, Highly ordered platinum-nanotubule arrays for amperometric glucose sensing, Adv. Funct. Mater. 15 (2005) 803-809.
17) O.K. Varghese, D. Gong, W.R. Dreschel, K.G. Ong, C.A. Grimes, Ammonia detection using nanoporous alumina resistive and surface acoustic wave sensors, Sens. Actuator B-Chem. 94 (2003) 27-35.
18) L. Wang, M. Sakurai, H. Kameyama, Study of catalytic decomposition of formaldehyde on Pt/TiO_2 alumite catalyst at ambient temperature, J. Hazard. Mater. 167 (2009) 399-405.
19) L. Wang, M. Sakurai, H. Kameyama, Catalytic oxidation of dichloromethane and toluene over platinum alumite catalyst, J. Hazard. Mater. 154 (2008) 390-395.
20) L. Wang, Q. Zhang, M. Sakurai, H. Kameyama, Development of a Pt/TiO_2 catalyst on an anodic alumite film for catalytic decomposition of formaldehyde at room temperature, Catal. Commun. 8 (2007) 2171-2175.
21) F. Zhou, A.K.M. Al-Zenati, A. Baron-Wiecheć, M. Curioni, S.J. Garcia-Vergara, H. Habazaki, P. Skeldon, G.E. Thompson, Volume expansion factor and growth efficiency of anodic alumina formed in sulphuric acid, J. Electrochem. Soc. 158 (2011) C202-C214.
22) M. Michalska-Domańska, M. Norek, W.J. Stępniowski, B. Budner, Fabrication of high quality anodic aluminum oxide (AAO) on low purity aluminum—A comparative study with the AAO produced on high purity aluminum, Electrochim. Acta 105 (2013) 424-432.
23) S. Stojadinovic, R. Vasilic, I. Belca, M. Tadic, B. Kasalica, L. Zekovic, Structural and luminescence characterization of porous anodic oxide films on aluminum formed in sulfamic acid solution, Appl. Surf. Sci. 255 (2008) 2845-2850.
24) O. Nishinaga, T. Kikuchi, S. Natsui, R.O. Suzuki, Rapid fabrication of self-ordered porous alumina with 10-/sub-10-nm-scale nanostructures by selenic acid anodizing, Sci. Rep. 3 (2013) 2748.
25) T. Kikuchi, O. Nishinaga, S. Natsui, R.O. Suzuki, Self-ordering behavior of anodic porous alumina via selenic acid anodizing, Electrochim. Acta 137 (2014) 728–735.
26) A. Baron-Wiecheć, M.G. Burke, T. Hashimoto, H. Liu, P. Skeldon, G.E. Thompson,

H. Habazaki, J.-J. Ganem, I.C. Vickridge, Tracer study of pore initiation in anodic alumina formed in phosphoric acid, Electrochim. Acta 113 (2013) 302-312.
27) X. Zhu, Y. Song, D. Yu, C. Zhang, W. Yao, A novel nanostructure fabricated by an improved two-step anodizing technology, Electrochem. Commun. 29 (2013) 71-74.
28) W.J. Stępniowski, M. Norek, M. Michalska-Domańska, A. Bombalska, A. Nowak-Stępniowska, M. Kwaśny, Z. Bojar, Fabrication of anodic aluminum oxide with incorporated chromate ions, Appl. Surf. Sci. 259 (2012) 324-330.
29) W.J. Stępniowski, M. Michalska-Domańska, M. Norek, T. Czujko, Fast Fourier transform based arrangement analysis of poorly organized alumina nanopores formed via self-organized anodization in chromic acid, Mater. Lett. 117 (2014) 69-73.
30) L. Zaraska, W.J. Stępniowski, E. Ciepiela, G.D. Sulka, The effect of anodizing temperature on structural features and hexagonal arrangement of nanopores in alumina synthesized by two-step anodizing in oxalic acid, Thin Solid Films 534 (2013) 155-161.
31) B. Sun, J. Li, X. Jin, C. Zhou, Q. Hao, X. Gao, Self-ordered hard anodization in malonic acid and its application in tailoring alumina taper-nanopores with continuously tunable periods in the range of 290–490nm, Electrochim. Acta 112 (2013) 327-332.
32) I.A. Vrublevsky, K.V. Chernyakova, A. Ispas, A. Bund, S. Zavadski, Optical properties of thin anodic alumina membranes formed in a solution of tartaric acid, Thin Solid Films 556 (2014) 230-235.
33) S.Z. Chu, K. Wada, S. Inoue, M. Isogai, Y. Katsuta, A. Yasumori, Large-scale fabrication of ordered nanoporous alumina films with arbitrary pore intervals by critical-potential anodization, J. Electrochem. Soc. 153 (2006) B384-B391.
34) M. Pashchanka, J. Schneider, Experimental validation of the novel theory explaining self-organization in porous anodic alumina films, Phys. Chem. Chem. Phys. 15 (2013) 7070-7074.
35) Y. Katsuta, A. Yasumori, K. Wada, K. Kurashima, S. Suehara, S. Inoue, Three-dimensionally nanostructured alumina film on glass substrate: Anodization of glass surface, J. Non-Cryst. Solids 354 (2008) 451-455.
36) T. Kikuchi, T. Yamamoto, R.O. Suzuki, Growth behavior of anodic porous alumina formed in malic acid solution, Appl. Surf. Sci. 284 (2013) 907-913.
37) T. Fukushima, Y. Fukuda, G. Ito, Y. Sato, Anodic oxidation of local corrosion of aluminum in mono-carboxylic acids, J. Surf. Fin. Soc. Jpn. 21 (1970) 319-326.
38) D. Nakajima, T. Kikuchi, S. Natsui, R.O. Suzuki, Growth behavior of anodic oxide formed by aluminum anodizing in glutaric and its derivative acid electrolytes, Appl. Surf. Sci. 321 (2014) 364-370.
39) T. Kikuchi, O. Nishinaga, S. Natsui, R.O. Suzuki, Fabrication of anodic porous alumina via acetylenedicarboxylic acid anodizing, ECS Electrochem. Lett. 3 (2014) C25-C28.
40) T. Kikuchi, T. Yamamoto, S. Natsui, R.O. Suzuki, Fabrication of anodic porous

alumina by squaric acid anodizing, Electrochim. Acta 123 (2014) 14–22.
41) T. Kikuchi, D. Nakajima, J. Kawashima, S. Natsui, R.O. Suzuki, Fabrication of anodic porous alumina via anodizing in cyclic oxocarbon acids, Appl. Surf. Sci. 313 (2014) 276–285.
42) W. Lee, R. Ji, U. Gösele, K. Nielsch, Fast fabrication of long-range ordered porous alumina membranes by hard anodization, Nat. Mater. 5 (2006) 741-747.
43) T. Kikuchi, O. Nishinaga, S. Natsui, R.O. Suzuki, Fabrication of Self-Ordered Porous Alumina via Etidronic Acid Anodizing and Structural Color Generation from Submicrometer-Scale Dimple Array, Electrochim. Acta 156 (2015) 235-243.
44) P. Kim, W.E. Adorno-Martinez, M. Khan, J. Aizenberg, Enriching libraries of high-aspect-ratio micro-or nanostructures by rapid, low-cost, benchtop nanofabrication, Nat. Protoc. 7 (2012) 311-327.
45) D. Losic, J.G. Mitchell, R. Lal, N.H. Voelcker, Rapid Fabrication of Micro-and Nanoscale Patterns by Replica Molding from Diatom Biosilica, Adv. Funct. Mater. 17 (2007) 2439-2446.
46) R.N.A. Prebiotic, Polymer microstructures formed by moulding in capillaries, Nature 376 (1995) 581-584.
47) I. Turkevych, V. Ryukhtin, V. Garamus, S. Kato, T. Takamasu, G. Kido, M. Kondo, Studies of self-organization processes in nanoporous alumina membranes by small-angle neutron scattering, Nanotechnology 23 (2012) 325606.
48) K. Chung, S. Yu, C.-J. Heo, J.W. Shim, S.-M. Yang, M.G. Han, H.-S. Lee, Y. Jin, S.Y. Lee, N. Park, J.H. Shin, Flexible, angle-independent, structural color reflectors inspired by morpho butterfly wings, Adv. Mater. 24 (2012) 2375-2379.
49) Y. Zhao, Z. Xie, H. Gu, C. Zhu, Z. Gu, Bio-inspired variable color materials, Chem. Soc. Rev. 41 (2012) 3297-3317.
50) H.J. Lezec, J.J. McMahon, O. Nalamasu, P.M. Ajayan, Submicrometer dimple array based interference color field displays and sensors, Nano Lett. 7 (2007) 329-333.
51) C. Lin, L.J. Martínez, M.L. Povinelli, Fabrication of transferrable, fully suspended silicon photonic crystal nanomembranes exhibiting vivid structural color and high-Q guided resonance, J. Vac. Sci. Technol. B 31 (2013) 050606.
52) J. Qu, D. Nie, C. Liu, H. Wang, G. Chen, Self-assembling behavior of TDPA molecules on inhomogeneous surface of 2024 aluminum alloy, Suf. Interface Anal. 45 (2013) 1363-1371.
53) K. Nakayama, E. Tsuji, Y. Aoki, H. Habazaki, Fabrication of superoleophobic hierarchical surfaces for low-surface-tension liquids, RSC Adv. 4 (2014) 30927-30933.

Captions

Fig. 1 Changes in current density, j, with anodizing time, t, in a 0.3 M etidronic acid solution at a) U = 210 V and T = 313 K, b) 240 V and 298 K, and c) 270 V and 293 K. Each set of anodizing conditions, including voltage, temperature, and time, was selected for fabrication of highly ordered anodic porous alumina.

Fig. 2 Surface appearances of the nanostructured aluminum specimens after anodizing in a) through c) etidronic acid and d) ketoglutaric acid. The anodized specimens were immersed in a CrO_3/H_3PO_4 solution to completely dissolve the anodic oxide.

Fig. 3 SEM images of the highly ordered aluminum dimple arrays with different periods, as shown in Fig. 2a through 2c.

Fig. 4 SEM image of the disordered dimple array formed on the aluminum surface by anodizing with ketoglutaric acid, as shown in Fig. 2d.

Fig. 5 Reflection spectrums from the a) electropolished and b) nanostructured aluminum surfaces formed by anodizing with ketoglutaric acid (Fig. 4) at different angles under white light irradiation.

Fig. 6 Reflection spectrums of the nanostructured aluminum surfaces formed by anodizing with etidronic acid a) at U = 210 V for D = 530 nm, b) at 240 V for 600 nm, and c) at 270 V for 670 nm. SEM images of the nanostructured aluminum surface at different angles of 0° and 50.0° are shown in Fig. 6d and 6e.

Fig. 7 Surface appearances of the a) electropolished and b) nanostructured 5.0-mm and 10.0-mm diameter aluminum rods.

Fig. 8 Photographs of the nanoimprints for the transfer of structural coloration. a) TDPA-SAM coating on the aluminum surface. b) Curing of the PDMS with the nanostructured aluminum specimen in a Petri dish. c) Removal of the nanostructured aluminum specimen from the cured PDMS. d) Cutting the edges of the PDMS negative mold, applying a UV curing photopolymer on the PDMS mold, and subsequently irradiating using UV light through a glass slide. e) Removal of the curable polymer from the PDMS mold. f) Coating of a platinum thin layer on the curable polymer via magnetron sputtering.

Fig. 9 SEM image of a) the nanostructured aluminum surface removed from the PDMS negative mold and b) the UV curable photopolymer fabricated by nanoimprinting.

Fig. 10 Reflection spectrums from the UV-curable polymer surface a) without and b) with the platinum coating. c) Reflection spectrums from the backside of the platinum-coated polymer replicas.

Fig. 11 Surface appearances of the nanostructured a) PDMS/TiO_2 nanoparticles and b) PDMS/MWCNT composites.

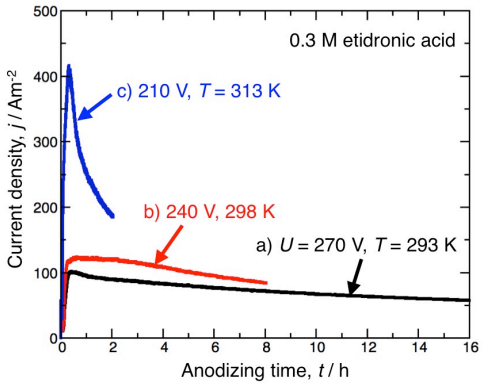
0.3 M etidronic acid
c) 210 V, T = 313 K
b) 240 V, 298 K
a) U = 270 V, T = 293 K
Current density, j / Am-2
Anodizing time, t / h
0
100
200
300
400
500
0
2
4
6
8
10
12
14
16

Fig. 1

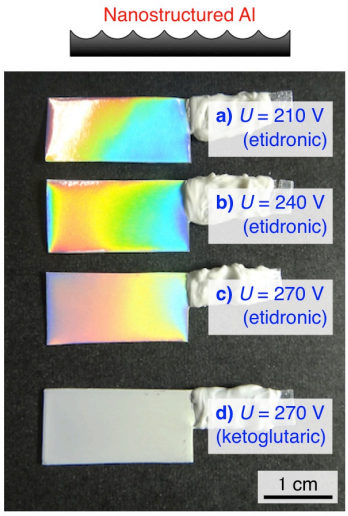
Nanostructured Al
a) U = 210 V
(etidronic)
b) U = 240 V
(etidronic)
c) U = 270 V
(etidronic)
d) U = 270 V
(ketoglutaric)
1 cm

Fig. 2

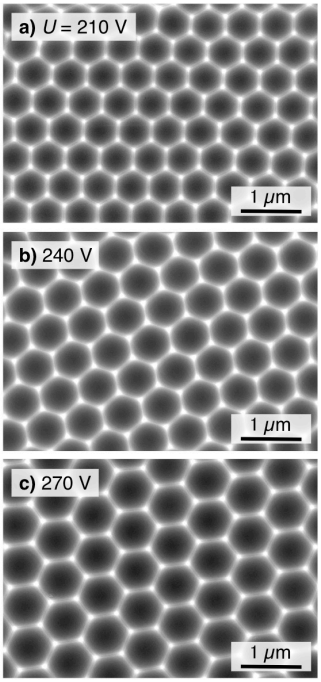

Fig. 3

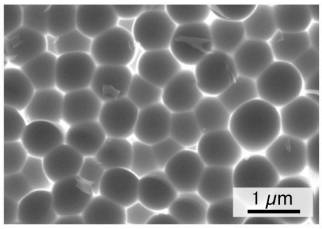

Fig. 4

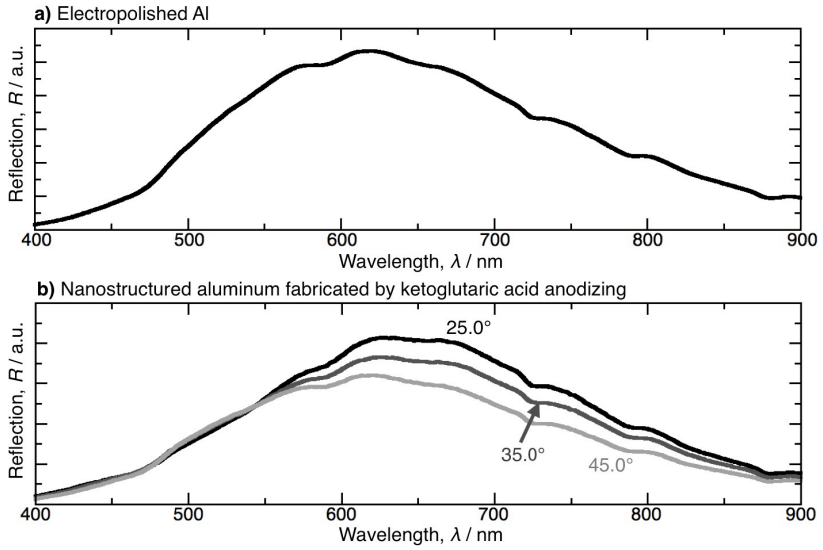
a) Electropolished Al
Reflection, R / a.u.
400
500
600
700
800
900
Wavelength, λ / nm
b) Nanostructured aluminum fabricated by ketoglutaric acid anodizing
Reflection, R / a.u.
25.0°
35.0°
45.0°
400
500
600
700
800
900
Wavelength, λ / nm

Fig. 5

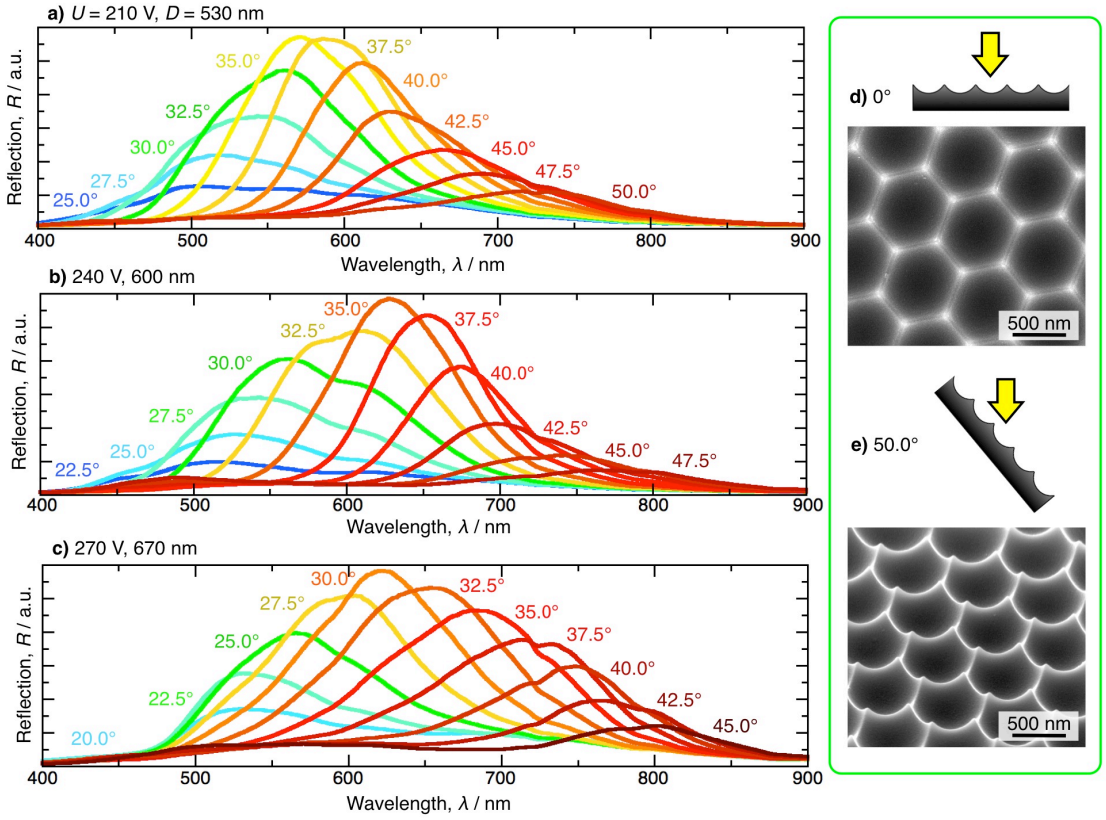
a) U = 210 V, D = 530 nm
Reflection, R / a.u.
Wavelength, λ / nm
25.0°
27.5°
30.0°
32.5°
35.0°
37.5°
40.0°
42.5°
45.0°
47.5°
50.0°
b) 240 V, 600 nm
22.5°
25.0°
27.5°
30.0°
32.5°
35.0°
37.5°
40.0°
42.5°
45.0°
47.5°
c) 270 V, 670 nm
20.0°
22.5°
25.0°
27.5°
30.0°
32.5°
35.0°
37.5°
40.0°
42.5°
45.0°
d) 0°
500 nm
e) 50.0°
500 nm

Fig. 6

Fig. 7

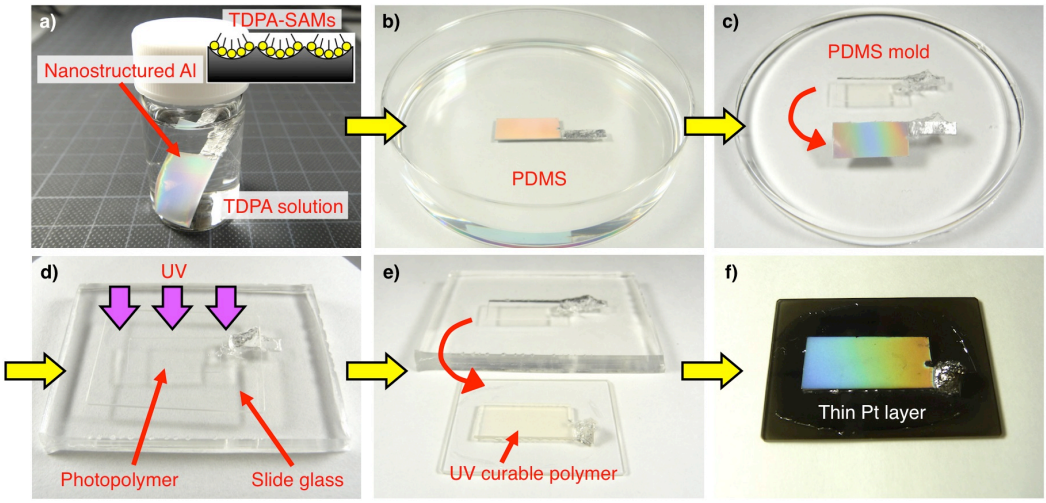
a)
TDPA-SAMs
Nanostructured Al
TDPA solution
b)
PDMS
c)
PDMS mold
d)
UV
Photopolymer
Slide glass
e)
UV curable polymer
f)
Thin Pt layer

Fig. 8

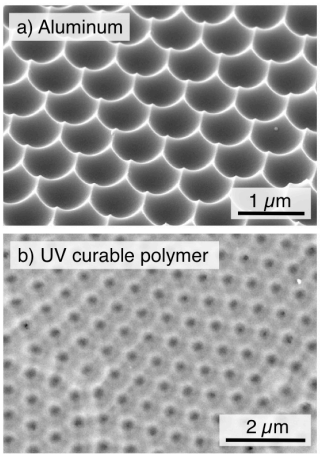

Fig. 9

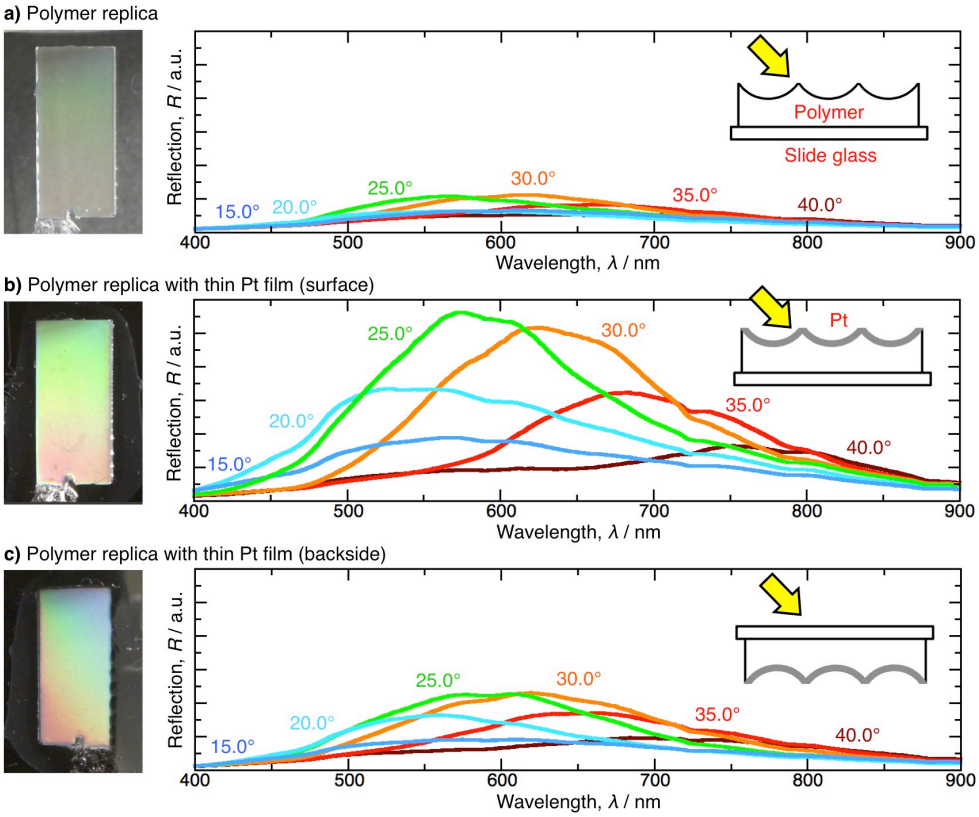
a) Polymer replica
Reflection, R / a.u.
Polymer
Slide glass
15.0°
20.0°
25.0°
30.0°
35.0°
40.0°
400
500
600
700
800
900
Wavelength, λ / nm
b) Polymer replica with thin Pt film (surface)
Reflection, R / a.u.
Pt
15.0°
20.0°
25.0°
30.0°
35.0°
40.0°
400
500
600
700
800
900
Wavelength, λ / nm
c) Polymer replica with thin Pt film (backside)
Reflection, R / a.u.
15.0°
20.0°
25.0°
30.0°
35.0°
40.0°
400
500
600
700
800
900
Wavelength, λ / nm

Fig. 10

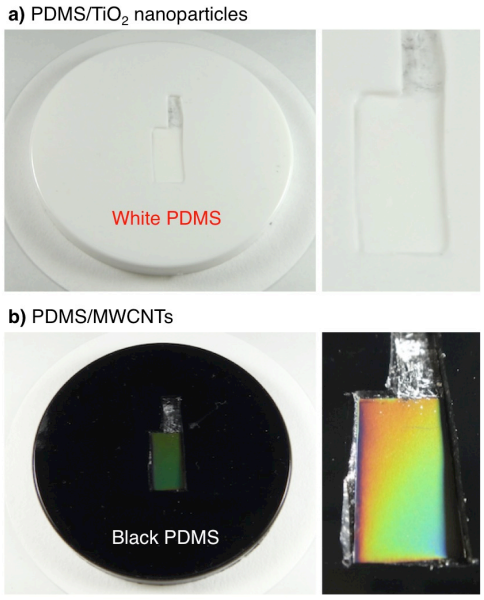
a) PDMS/TiO2 nanoparticles
White PDMS
b) PDMS/MWCNTs
Black PDMS

Fig. 11